Alpha-induced reaction cross-section for Sm, U, Np targets: influence of hexadecapole deformation and deformed surface diffuseness

S. A. Alavi[1)] V. Dehghani[2)]

Department of Physics, University of Sistan and Baluchestan, Zahedan 98135-674, Iran

Abstract: Alpha-induced reactions on ^{154}Sm, ^{233,235,236,238}U, and ^{237}Np deformed nuclei are studied theoretically. The effects of hexadecapole deformation, deformed surface diffuseness parameter, and orientation on barrier height and position, fusion cross-section at any angle, and fusion cross-section have been investigated. Both hexadecapole deformation and deformed surface diffuseness can affect barrier characteristics and enhance fusion cross-section. Good agreement between experimental data and theoretical calculations with quadrupole and hexadecapole deformation and deformed surface diffuseness were observed for the ^{4}He+^{154}Sm, ^{235}U, ^{237}Np reactions.

Keywords: nuclear potential, fusion cross section, deformation, alpha induced reaction.

PACS: 25.70.Jj, 24.10.-i **DOI:** 10.1088/1674-1137/41/6/064104

1 Introduction

Because of the great importance and many applications of alpha-induced reactions, they have been the subject of many experimental and theoretical investigations [1–4]. From the theoretical point of view, in alpha-induced reactions on deformed heavy target nuclei, the choice of proper nuclear interaction potential and the inclusion of nuclear deformation in the effective interaction potential is essential. The proximity potential, which is based on the proximity force theorem [5, 6], is one of the widely used nuclear interaction potentials. Some well known forms of the proximity potential are Proximity 77 (prox 77) [7], Proximity 88 (prox 88) [8, 9], Proximity 2000 (prox 00) [10], Bass 80 [11], Broglia-Winther (BW91) [9, 12], and Denisov DP [5]. By considering nuclear deformation up to hexadecapole (β_4), the effect of these proximity potentials on barrier characteristics and fusion dynamics have been studied for 52 fusion reactions with deformed target or projectile nuclei in Ref. [13]. The strong dependence of some heavy ion and superheavy fusion reaction dynamics on the nuclear hexadecapole deformation have been investigated in Refs. [14–19]. The Broglia-Winther nuclear proximity potential (BW91) is in the form of the Woods-Saxon potential and strictly depends on the surface diffuseness parameter. Initial formulae for deformed surface diffuseness of spheroid nuclei have been given in Refs. [20–22]. However, a more accurate and corrected form of the deformed surface diffuseness formula has been introduced in [23, 24]. Reference [25] showed that small variations in the choice of constant values of surface diffuseness noticeably influence fusion dynamics. Therefore, one may expect the inclusion of the deformed surface diffuseness in fusion dynamics calculations to have a significant effect.

In order to calculate the barrier characteristics and fusion cross section and compare the obtained results for two cases, 1) constant and deformed surface diffuseness, and 2) deformation up to hexadecapole (β_4), we have employed the deformed Wong formula [26]. For more details about the Wong formula see Refs. [13, 27, 28].

In this paper, our aim is to investigate the role of hexadecapole deformation and deformed surface diffuseness in fusion dynamics. In Section 2, the fusion cross-section is introduced by considering the effective potential as the sum of the deformed BW91 nuclear potential with deformed surface diffuseness and the deformed Coulomb potential. The obtained results for ^{4}He+^{154}Sm, ^{233,235,236,238}U, ^{237}Np reactions are given in Section 3. Finally, concluding remarks are given in Section 4.

2 Fusion cross-section

For deformed nuclei, the analytic fusion cross-section formula at each angle is calculated using the Wong formula at zero nuclear temperature as [26, 27, 29]

$$\sigma_{\rm fus}(E_{\rm cm},\theta)=\frac{R_{\rm B}^2\hbar\omega_0}{2E_{\rm cm}}\ln\left[1+{\rm e}^{\frac{2\pi}{\hbar\omega_0}(E_{\rm cm}-V_{\rm B})}\right], \quad (1)$$

Received 28 January 2017

1) E-mail: s.a.alavi@phys.usb.ac.ir

2) E-mail: vdehghani@phys.usb.ac.ir

where $V_{\rm B} = V_{\rm B}(\theta)$, $R_{\rm B} = R_{\rm B}(\theta)$, and $\hbar\omega_0$ are barrier height, corresponding barrier position, and curvature of potential, respectively. These parameters are obtained based on the Hill-Wheeler [30] approximation for assimilating the shape of the effective interaction barrier potential $V(r,\theta)$ through an inverted harmonic oscillator

$$V(r,\theta) = V_{\rm B}(\theta) - \frac{1}{2}\mu\omega_0^2(r-R_{\rm B})^2. \tag{2}$$

The barrier position $R_{\rm B}$ is calculated by

$$\frac{{\rm d}V(r)}{{\rm d}r}|_{r=R_{\rm B}} = 0, \tag{3}$$

and consequently, the barrier height $V_{\rm B} = V(r = R_{\rm B},\theta)$ is obtained. The curvature $\hbar\omega_0$ is calculated as

$$\hbar\omega_0 = \frac{\hbar}{\sqrt{\mu}}\sqrt{\left|\frac{{\rm d}^2V(r)}{{\rm d}r^2}\right|_{r=R_{\rm B}}}. \tag{4}$$

The fusion cross-section can be obtained by integrating $\sigma_{\rm fus}(E_{\rm cm},\theta)$ over the orientation angles θ, as [31, 32]

$$\sigma_{\rm fus}(E_{\rm cm}) = \int_{\theta=0}^{\pi/2}\sigma_{\rm fus}(E_{\rm cm},\theta)\sin\theta{\rm d}\theta. \tag{5}$$

The explicit dependency of the barrier position on the deformed surface diffuseness makes barrier heights, curvature, and fusion cross section dependent on this parameter.

One of the recent parametrization of fusion barriers, which has been obtained by considering more than 200 reactions for projectiles/targets with masses between 6 and 238, is given as [33]

$$V_{\rm B}^{\rm emp.} = -1.01 + 0.93\times\frac{Z_{\rm p}Z_{\rm t}}{A_{\rm p}^{1/3}+A_{\rm t}^{1/3}} + (4.53\times10^{-4})\times\left(\frac{Z_{\rm p}Z_{\rm t}}{A_{\rm p}^{1/3}+A_{\rm t}^{1/3}}\right)^2. \tag{6}$$

The empirical formula for the fusion barrier positions is given as [33]

$$R_{\rm B}^{\rm emp.} = 3.58+0.88\times\left(A_{\rm p}^{1/3}+A_{\rm t}^{1/3}\right)+30\times\beta_3+0.4\times\left(\frac{N}{Z}-1\right), \tag{7}$$

where $\beta_3 = \beta_{3p}+\beta_{3t}$ and $\dfrac{N}{Z} = \dfrac{N_{\rm p}+N_{\rm t}}{Z_{\rm p}+Z_{\rm t}}$ correspond to octupole deformation and isospin content, respectively. However, the octupole deformation of the studied nuclei is zero.

In order to analyse the dependence of fusion cross-section on the deformed surface diffuseness parameter and hexadecapole deformation, we define the respective percentage differences of the fusion cross-section as

$$\Delta\sigma_{1,\rm fus}(\%) = \frac{\sigma_{\rm fus}^{a(\theta)}(E_{\rm cm})-\sigma_{\rm fus}^{a(0)}(E_{\rm cm})}{\sigma_{\rm fus}^{a(\theta)}(E_{\rm cm})}\times100, \tag{8}$$

$$\Delta\sigma_{2,\rm fus}(\%) = \frac{\sigma_{\rm fus}^{\beta_2,\beta_4}(E_{\rm cm})-\sigma_{\rm fus}^{\beta_2}(E_{\rm cm})}{\sigma_{\rm fus}^{\beta_2,\beta_4}(E_{\rm cm})}\times100, \tag{9}$$

where $\sigma_{\rm fus}^{a(\theta)}$ and $\sigma_{\rm fus}^{a(0)}$ are the fusion cross-sections with deformed and constant surface diffuseness, respectively, and $\sigma_{\rm fus}^{\beta_2,\beta_4}(E_{\rm cm})$ and $\sigma_{\rm fus}^{\beta_2}(E_{\rm cm})$ are the fusion cross-sections (with deformed surface diffuseness) with and without hexadecapole deformation, respectively.

The effective interaction barrier potential $V(r,\theta)$ in Eq. (2), including the attractive nuclear potential $V_{\rm N}(r,\theta)$, and repulsive Coulomb potential $V_{\rm C}(r,\theta)$, with $l=0$ is given by

$$V(r,\theta) = V_{\rm N}(r,\theta)+V_{\rm C}(r,\theta), \tag{10}$$

where θ is the orientation angle.

The deformed Broglia-Winther nuclear potential (BW91) $V_{\rm N}$ is written as

$$V_{\rm N}(r,\theta) = -\frac{V_0}{1+{\rm e}^{(r-R)/a}}. \tag{11}$$

The depth V_0 is given as

$$V_0 = 16\pi\overline{R}\gamma_0 a, \tag{12}$$

where surface energy constant for a spherical projectile is $\gamma_0 = 0.95$ MeV·fm^{-2}. The deformed surface diffuseness parameters $a = a(\theta)$ for actinides at $0\leqslant\theta\leqslant\pi/2$ is given as [24]

$$a(\theta) = a(0)+0.45\sin^2\theta-0.4\sin^3\theta, \tag{13}$$

and for rare-earth nuclei

$$a(\theta) = a(0)+0.25\sin^2\theta-0.25\sin^3\theta. \tag{14}$$

The constant value of surface diffuseness parameters is considered as $a(0) = 0.63$ (fm) [24]. The nuclear interaction potential radius R is given as

$$R = R_{\rm p}+R_{\rm t}+0.29({\rm fm}), \tag{15}$$

where

$$R_{\rm i} = (1.233A_{\rm i}^{1/3}-0.98A_{\rm i}^{-1/3})(1+\beta_{2\rm i}Y_{20}+\beta_{4\rm i}Y_{40}); {\rm i} = {\rm p},{\rm t}. \tag{16}$$

p and t signify projectile and target, respectively. The coefficients β_2, β_4 are quadrupole and hexadecapole deformation parameters of the deformed target nuclei, respectively. These parameters are taken from Ref. [34]. Mean curvature radius is approximately given as

$$\overline{R} \simeq \frac{R_{\rm p}R_{\rm t}}{R_{\rm p}+R_{\rm t}}. \tag{17}$$

The deformed Coulomb potential $V_{\rm C}$ is written as

$$V_{\rm C}(r,\theta) = \frac{1}{4\pi\varepsilon_0}\frac{Z_{\rm p}Z_{\rm t}e^2}{r}\cdot\left[1+\frac{3R^2(\theta)}{5r^2}\beta_2Y_{20}+\frac{3R^4(\theta)}{9r^4}\beta_4Y_{40}\right], \tag{18}$$

where $Z_{\rm p}$ and $Z_{\rm t}$ are the atomic number of projectile and target, respectively.

3 Results

The model described in the previous section is now applied to obtain the effect of deformed surface diffuseness and hexadecapole deformation on barrier characteristics and fusion cross section.

The fusion barrier characteristics of ^{4}He+^{154}Sm, ^{233,235,236,238}U, ^{237}Np reactions are shown in Table 1. Barrier heights $V_{\rm B}^{a0}$ and barrier position $R_{\rm B}^{a0}$ with constant surface diffuseness, barrier heights $V_{\rm B}^{a(\theta)}$ and barrier position $R_{\rm B}^{a(\theta)}$ with deformed surface diffuseness, and empirical barrier heights (position) $V_{\rm B}^{\rm emp.}$ ($R_{\rm B}^{\rm emp.}$) are listed in Table 1. The fusion barrier heights and positions have been calculated with optimum orientations. The details of optimum orientation have been given in Ref. [35]. Here, the barrier characteristics have been calculated for a hot configuration. Significant difference was seen between calculated barrier position and height using deformed and constant surface diffuseness. Because of the form of the deformed surface diffuseness formula for the lanthanide target ^{154}Sm, the same results have been obtained for the optimum orientation hot fusion configuration.

Table 1. Fusion barrier heights (in MeV) and barrier positions (in fm) with optimum orientations.

reaction	(β_2,β_4) [34]	$V_{\rm B}^{a0}$	$R_{\rm B}^{a0}$	$V_{\rm B}^{a(\theta)}$	$R_{\rm B}^{a(\theta)}$	$V_{\rm B}^{\rm emp.}$ [33]	$R_{\rm B}^{\rm emp.}$ [33]
^{4}He+ ^{154}Sm	(0.270, 0.105)	16.71	9.82	16.71	9.82	15.73	9.88
^{4}He+ ^{233}U	(0.206, 0.116)	22.70	10.82	22.25	11.00	21.35	10.60
^{16}O+ ^{235}U	(0.215, 0.106)	22.73	10.79	22.78	10.97	21.30	10.62
^{4}He+ ^{236}U	(0.226, 0.108)	22.73	10.78	22.28	10.96	21.28	10.64
^{4}He+ ^{238}U	(0.236, 0.098)	22.76	10.76	22.32	10.94	21.22	10.66
^{4}He+ ^{237}Np	(0.226, 0.108)	22.97	10.79	22.52	10.97	21.50	10.64

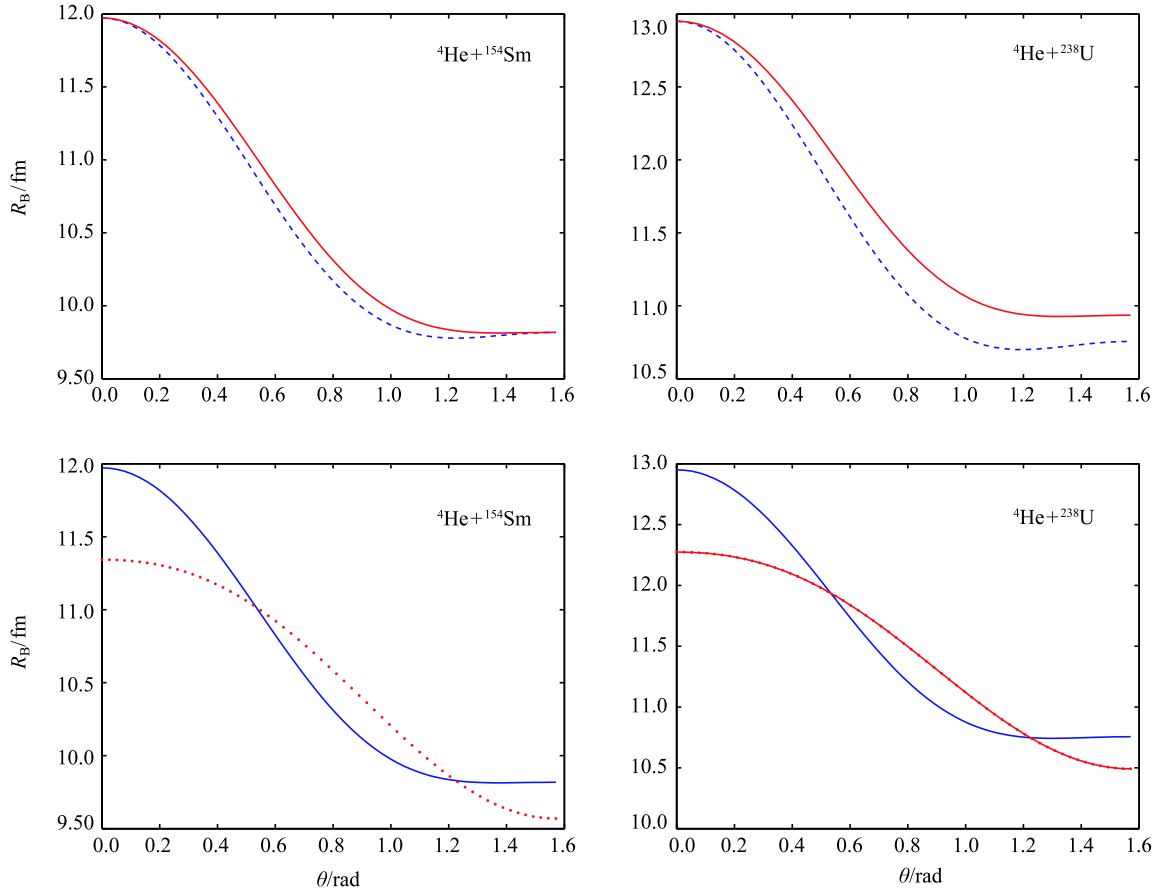

Fig. 1. (color online) (Upper panel) Barrier position as function of θ for ^{4}He+^{154}Sm and ^{4}He+^{238}U for both deformed (solid line) and constant (dashed line) surface diffuseness. (Lower panel) Barrier position with β_4 (solid line) and without β_4 (dashed line). Lower panel figures were plotted with deformed surface diffuseness.

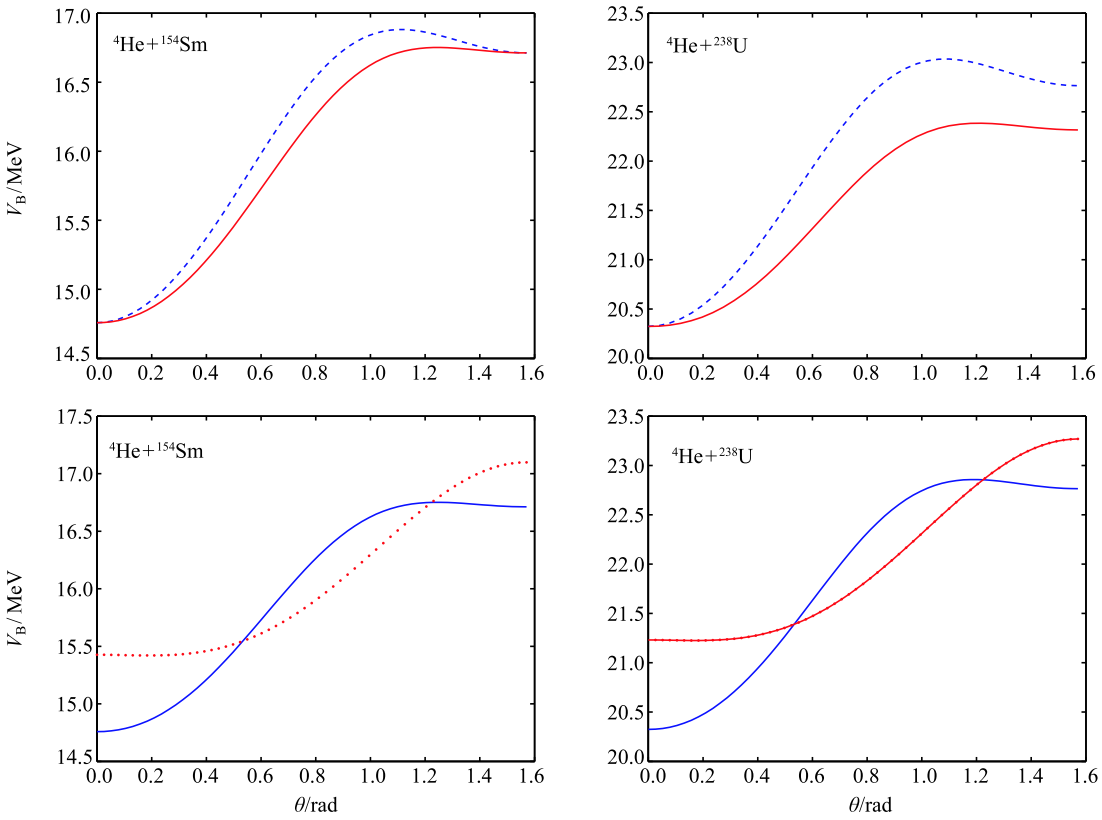

Fig. 2. (color online) Same as Fig. 1 but for barrier height.

The upper panels of Figs. 1 and 2 display the variations of barrier position and barrier height respectively for ^{4}He+^{154}Sm and ^{4}He+^{238}U reactions as a function of θ for both deformed and constant surface diffuseness. The variations of barrier position with and without hexadecapole deformation, by inclusion of deformed surface diffuseness, are shown in the lower panels. The obtained results show that by increasing the orientation θ the barrier position is decreased. Larger values are obtained for deformed surface diffuseness. However, this discrepancy is larger for ^{238}U actinide target nuclei than for ^{154}Sm lanthanide target nuclei. The reverse behavior is observed in barrier height calculations. Because of the form of the deformed surface diffuseness formula for lanthanides, the barrier position and barrier height at $\theta = \pi/2$, the optimum orientation angle for the hot configuration, are equal for both deformed and constant surface diffuseness, whereas the difference is noticeable at $\theta = \pi/2$ for actinide targets. The effect of hexadecapole deformation in calculation of barrier height and barrier position is significant and approximately the same for both ^{4}He+^{154}Sm and ^{4}He+^{238}U reactions.

Figure 3 shows the variation of fusion cross-section at each angle for the ^{4}He+^{154}Sm reaction at near-barrier and above-barrier energies E_{cm}=15 MeV and E_{cm}=22 MeV (upper panel), and the ^{4}He+^{238}U reaction at E_{cm}=23 MeV and E_{cm}=30 MeV (lower panel), as a function of the orientation angle for both deformed and constant surface diffuseness. With the increase of orientation angle, the fusion cross-section decreases smoothly. In comparison with constant surface diffuseness, deformed surface diffuseness gives larger values of fusion cross-section at each angle, especially at near-barrier energies. In order to analyze the variation of fusion cross-section at each angle and energy, three-dimensional plots are show in Fig. 4. The maximum of relative difference is reached around the lower energy and higher angles.

Figure 5 shows the variation of the calculated fusion cross-sections of ^{4}He+^{154}Sm, ^{4}He+^{233}U, ^{4}He+^{235}U ^{4}He+^{236}U, ^{4}He+^{238}U, and ^{4}He+^{237}Np reactions by considering deformed and constant surface diffuseness as a function of E_{cm}. The experimental fusion cross section data have been taken from Refs. [36–41]. The asterisks represent the experimental data. The dashed lines show the fusion cross-section with constant surface diffuseness. The obtained results show the significant effect of deformed surface diffuseness on fusion cross-section, especially near the barrier energy region. Inclusion of the deformed surface diffuseness gives larger values of fusion cross-section for alpha-induced reactions on prolate lanthanide and actinide target nuclei. In general,

good agreement between calculated fusion cross-section with deformed surface diffuseness and experimental fusion cross-section is observed for ^{4}He+^{154}Sm, ^{235}U, ^{237}Np reactions. Especially, nice coincidence is observed for ^{4}He+^{238}U and ^{4}He+^{237}Np reactions in the above-barrier energy region.

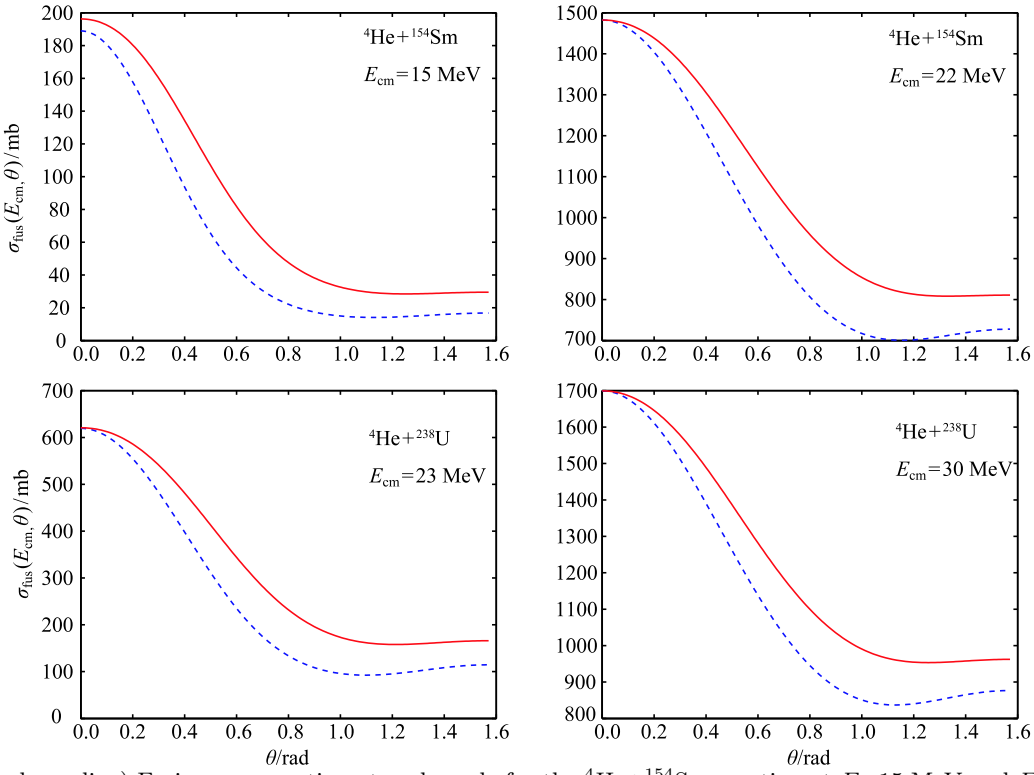

Fig. 3. (color online) Fusion cross-section at each angle for the ^{4}He+^{154}Sm reaction at E=15 MeV and E=22 MeV (upper panel) and the ^{4}He+^{238}U reaction at E=23 MeV and E=30 MeV (lower panel) as function of θ for both deformed (solid line) and constant surface diffuseness (dashed line).

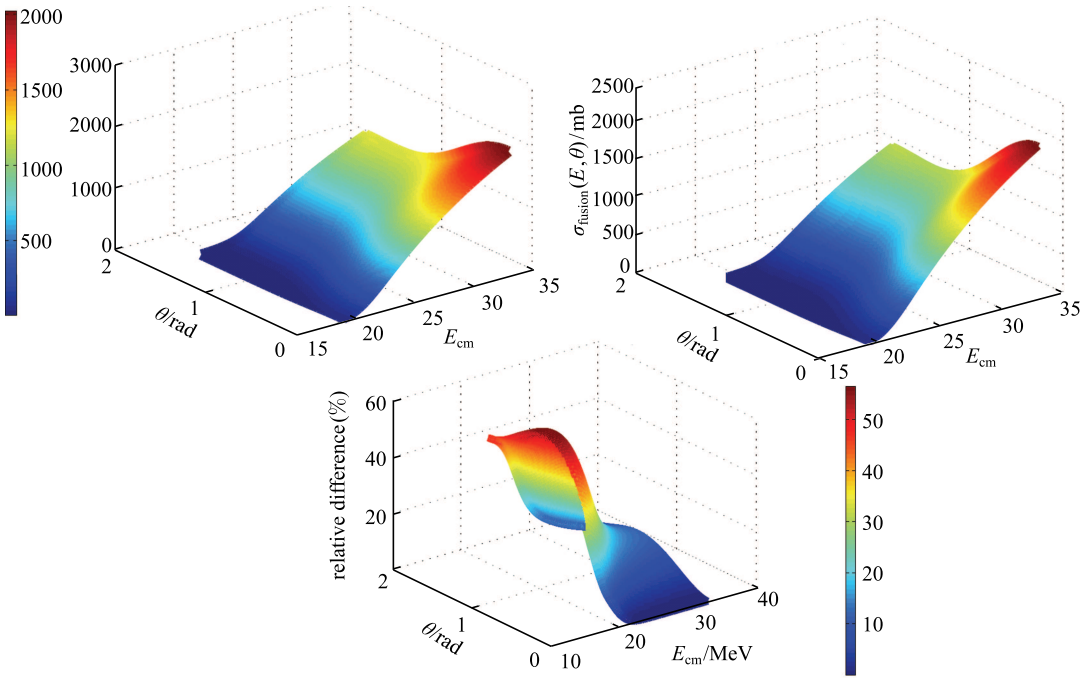

Fig. 4. (color online) Fusion cross-section at each angle and energy for the ^{4}He+^{238}U reaction as a function of θ and E for both deformed (left) and constant (right) surface diffuseness, and relative difference (bottom).

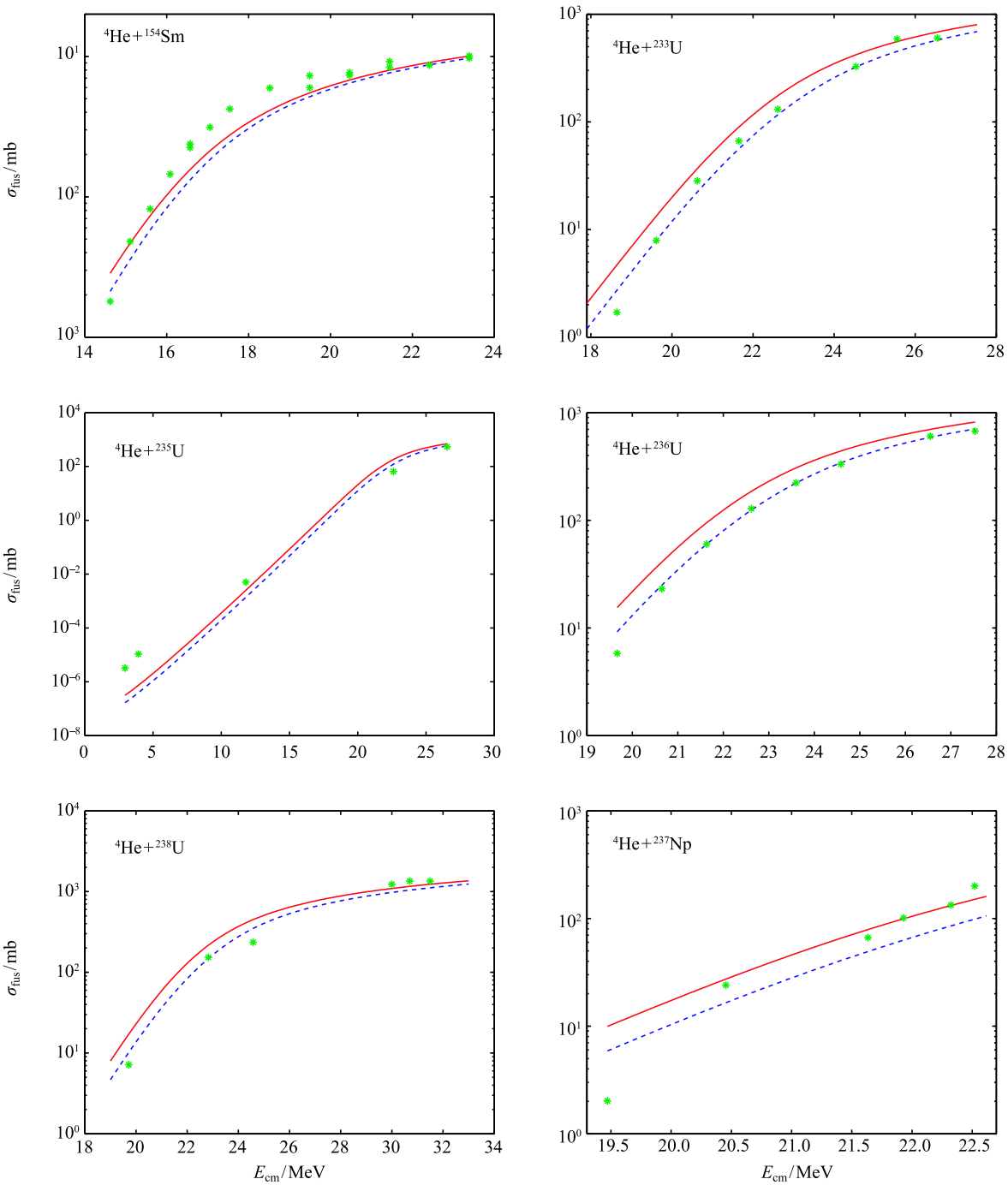

Fig. 5. (color online) Fusion cross-sections of the ^{4}He+^{154}Sm [36], ^{4}He+^{233}U [37], ^{4}He+^{233}U [38], ^{4}He+^{236}U [39], ^{4}He+^{238}U [40], and ^{4}He+^{237}Np [41] reactions as a function of E_{cm} with deformed and constant surface diffuseness. The dashed lines show the calculated fusion cross-sections with constant surface diffuseness.

Figure 6 shows the percentage difference of the calculated fusion cross-section with deformed and constant surface diffuseness for the ^{4}He+^{154}Sm and ^{4}He+^{238}U reactions. The percentage difference of the calculated fusion cross section with and without inclusion of hexadecapole deformation for the ^{4}He+^{154}Sm and ^{4}He+^{238}U reactions is displayed in Fig. 7. These figures show the large value of the percentage difference in the sub-barrier and near-barrier energy regions. In the above-barrier energy region this quantity falls off. Figure 7 shows that the effect of hexadecapole deformation on the fusion cross-sections of ^{4}He+^{154}Sm and ^{4}He+^{238}U reactions is noticeable, especially in the sub-barrier energy region.

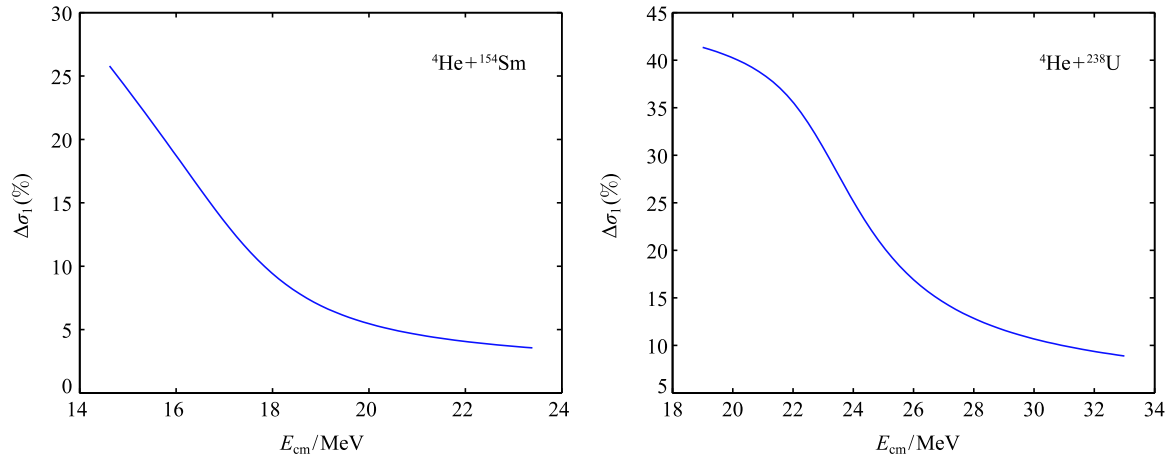

Fig. 6. (color online) Percentage difference of fusion cross-sections of the ^{4}He+^{154}Sm and ^{4}He+^{238}U reactions, as a function of E_{cm}, with deformed and constant surface diffuseness.

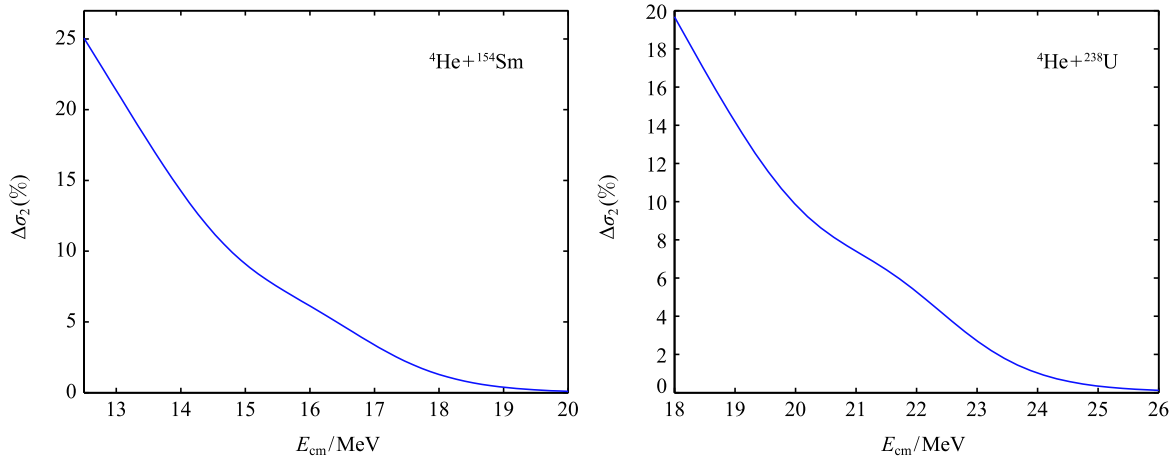

Fig. 7. (color online) Same as Fig. 6 but for percentage difference of the fusion cross-section with and without inclusion of hexadecapole deformation. Figures were plotted with deformed surface diffuseness.

4 Discussion and conclusion

In this theoretical investigation, by employing the Wong formula and considering a deformed Coulomb potential and deformed Broglia-Winther (BW91) nuclear interaction potential with deformed surface diffuseness parameter, the barrier position and height and fusion cross-sections of ^{4}He+^{154}Sm, ^{4}He+^{233}U, ^{4}He+^{235}U ^{4}He+^{236}U, ^{4}He+^{238}U, ^{4}He+^{237}Np reactions have been studied. We conclude that there is a significant effect from the deformed surface diffuseness and hexadecapole deformation parameter. In these alpha-induced reactions on prolate deformed target nuclei, the larger values of fusion cross-section were obtained by including deformed surface diffuseness and hexadecapole deformation parameter. Good agreement between experimental data and theoretical calculations with full deformation parameters were observed for the ^{4}He+^{154}Sm, ^{235}U, ^{237}Np reactions.

References

1 Wayne Swenson, Nikola Cindro, Phys. Rev., **123**: 910 (1961)
2 S. J. Iwata, J. Phys. Soc. Japan., **17**: 1323 (1962); S. Tanaka, M. Furukawa, T. Mikumo, S. Iwata, M. Yagi and H. Amano, J. Phys. Soc. Japan, **15**: 952 (1960)
3 P. Mohr, Eur. Phys. J. A, **51.5**: 1 (2015)
4 G. G. Kiss et al, Phys. Lett. B, **735** : 40 (2014)
5 V. Yu. Denisov, Phys. Lett. B, **526**: 315 (2002)
6 Ning Wang et al, Phys. Rev. C, **74**: 044604 (2006)
7 J. Blocki et al, Ann. Phys. (NY), **105**: 427 (1977)
8 P. Mller and J. R. Nix., Nucl. Phys. A, **361**: 117 (1981)
9 W. Reisdorf, J. Phys. G: Nucl. Part. Phys., **20**: 1297 (1994)
10 W. D. Myers and W. J. Sowiatecki, Phys. Rev. C, **62**: 044610 (2000)

11 R. Bass, Phys. Rev. Lett., **39**: 265 (1977)
12 P. R. Christensen and A. Winther, Phys. Lett. B, **65**: 19 (1976)
13 D. Jain, R. Kumar, and M. K. Sharma, Nucl. Phys. A, **915**: 106 (2013)
14 J. O. Fernandez Niello and C. H. Dasso, Phys. Rev. C, **39**: 2069 (1989)
15 M. J. Rhoades-Brown and V. E. Oberacker, Phys. Rev. Lett., **50**: 1435 (1983)
16 R. C. Lemmon et al, Phys. Lett. B, **316**: 32 (1993)
17 T. Rajbongshi et al, Phys. Rev. C, **93**: 054622 (2016)
18 X. J. Bao et al, J. Phys. G : Nucl. Part. Phys., **43**: 125105 (2016)
19 C. R. Morton et al, Phys. Rev. C, **64**: 034604 (2001)
20 A. Bohr and B. Mottelson, Nuclear Structure Vol. 2: Nuclear Deformations, World Scientific, Singapore, 1998
21 A. Saxena and V. S. Ramamurthy, Pramana J. Phys., **27**: 15 (1986)
22 B. S. Ishkhanov and V. N. Orlin, Phys. At. Nucl., **68**: 1352 (2005)
23 G. Scamps, D. Lacroix, G. G. Adamian and N. V. Antonenko, Phys. Rev. C, **88**: 064327 (2013)
24 G. G. Adamian, N. V. Antonenko, L. A. Malov, G. Scamps, and D. Lacroix, Phys. Rev. C, **90**: 034322 (2014)
25 I. Dutt and R. K. Puri, Phys. Rev. C, **81**: 047601 (2010)
26 C. Y. Wong, Phys. Rev. Lett., **31**: 766 (1973)
27 R. Kumar, M. Bansal, S. K. Arun and R. K. Gupta, Phys. Rev. C, **80**: 034618 (2009)
28 K. Hagino and N. Takigawa, Prog. Theor. Phys., **128**: 1061 (2012)
29 R. Kumar, Phys. Rev. C, **84**: 044613 (2011)
30 D. L. Hill and J. A. Wheeler, Phys. Rev., **89**: 1102 (1953); T. D. Thomas, ibid. **116**, 703 (1959)
31 Yibin Qian, Zhongzhou Ren and Dongdong Ni, Phys. Rev. C, **83**: 044317 (2011)
32 Yibin Qian and Zhongzhou Ren, Phys. Rev. C, **84**: 064307 (2011)
33 R. Kumari, R. K. Puri, Nucl. Phys. A, **933**: 135 (2015)
34 P. Mller, A. J. Sierk, T. Ichikawa, H. Sagawa, Atomic Data and Nuclear Data Tables, **109**: 1 (2016)
35 R. K. Gupta, M. Balasubramaniam, R. Kumar, N. Singh, M. Manhas and W. Greiner, J Phys. G: Nucl. Part. Phys., **31**: 631 (2005)
36 S. Gil et al, Phys. Rev. C, **31**: 1752 (1985)
37 H. Freiesleben, J. R. Huizenga, Nucl. Phys. A, **224**: 503 (1974)
38 N. N Ajitanand et al, Phys. Rev. C, **40**: 1854 (1989)
39 P. Limkilde, G. Sletten, Nucl. Phys. A, **199**: 504 (1973)
40 R. Raabe, J. L. Sida, J. L. Charvet et al, Nature, **431**: 823 (2004)
41 Alain Fleury, F. H. Ruddy, M. N. Namboodiri et al, Phys. Rev. C, **7**: 1231 (1973)